

# Effect of sparsity and exposure on total variation regularized X-ray tomography from few projections

Jakob S. Jørgensen\*, Sophia B. Coban†, William R.B. Lionheart† and Philip J. Withers†

**Abstract**—We address effects of exposure and image gradient sparsity for total variation-regularized reconstruction: is it better to collect many low-quality or few high-quality projections, and can gradient sparsity predict how many projections are necessary? Preliminary results suggest collecting many low-quality projections is favorable, and that a link may exist between gradient sparsity level and successful reconstruction.

## I. INTRODUCTION

Sparsity regularization for X-ray computed tomography (CT) image reconstruction, for example total variation (TV) regularization [1] for gradient-sparse images, has been seen to allow drastically reduced numbers of projections compared to conventional analytical methods, see, e.g. [2]. In medical imaging and non-destructive testing this may allow reduced X-ray exposure or data acquisition time. In today’s literature, there is little quantitative guidance on how much TV-regularization allows us to reduce the number of projections. In order for TV and other forms of sparsity regularization to become appropriately used this lack of knowledge must be filled. Our recent work [3] has indicated in simulations inspired by compressed sensing [4] that sparsity of the image gradient can predict how few projections will suffice for accurate TV-regularized reconstruction. A main goal of the present work is to investigate, for the first time, if the same argument holds using real X-ray CT data.

In the present study we consider exposure as the measurement cost, and – given a fixed total exposure – look at the trade off between more information obtained at lower quality (more projections at low exposure) and less information at higher quality (fewer projections at high exposure). The sparsity-regularization literature often takes number of projections as the primary variable, however the total exposure of a CT scan depends both on the number of projections and the exposure-per-projection. [2], [4]. So one could also reduce the total exposure by keeping the usual high number of projections but decreasing the exposure time of each. It is not immediately clear in which scenario TV-regularized reconstruction will perform better. Addressing this issue is the other main goal of this work.

In the present work we systematically study TV-regularized reconstruction quality at reduced numbers of projections as a function of both exposure time and gradient sparsity using real CT data. Specifically we address:

- Q1: Does TV-regularized reconstruction compensate better for reduced information from few high-exposure or many low-exposure projections?  
 Q2: Is there a connection between gradient sparsity and how few projections provide enough information that TV-regularized reconstruction succeeds?

While Q1 considers a fixed total exposure with exposure-per-projection inversely proportional to the number of projections, Q2 considers a constant exposure-per-projection and a total exposure proportional to the number of projections.

We will use the recently published SophiaBeads data set, which has been designed specifically for systematic studies of advanced reconstruction algorithms. In addition to using this data set to address the stated questions, we apply the present work to examine how appropriately the SophiaBeads data set can serve the purpose of testing sparsity-regularized reconstruction methods.

An important note needs to be made here about our definition of an ‘adequate reconstruction’. In our earlier work [3], we used a relative 2-norm measure to assess if reconstructions *perfectly* recovered the ground truth. This was appropriate for the idealized scenario and to stay consistent, we also report 2-norm errors in this work. However with real data, we wish to assess how well important features can be quantified; in this case known to be disk-shaped and we employ an aspect-ratio quality measure as explained in §IV-B.

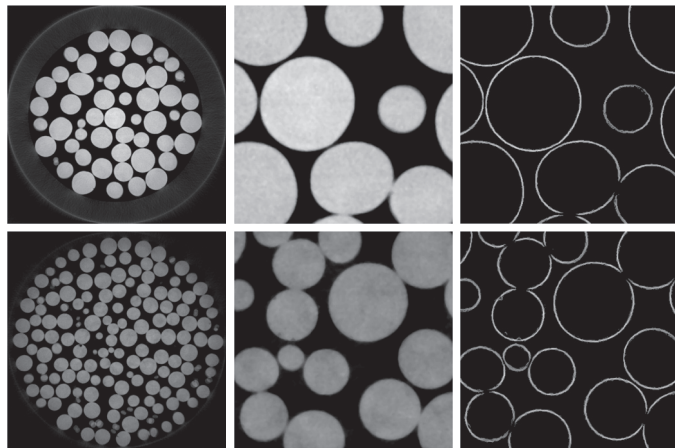


Fig. 1. Ground truths for SophiaBeads data sets S1 (top row) and S2 (bottom row) obtained by 30 CGLS iterations from pooled projections, followed by median filtering. Full  $1564 \times 1564$  images (left),  $350 \times 350$  region of interest around the centre (centre), and sparse thresholded gradient magnitude region of interests (right).

\*Technical University of Denmark, 2800 Kgs. Lyngby, Denmark.

†The University of Manchester, Manchester, M13 9PL, United Kingdom.  
 Corresponding author contact: jakj@dtu.dk.

II. TEST DATA

A. The SophiaBeads test data set

The SophiaBeads Dataset Project [5] is a collection of cone-beam X-ray CT data sets where the number of projections are varied while the total photon count (or the total exposure time) is kept constant, i.e. the exposure-per-projection is inversely proportional to the number of projections, as in Q1. This enables a wide range of algorithm comparisons and information content optimizations to be examined. For more detailed information on this experimental framework and the examples of such scenarios, we refer the reader to [6].

The SophiaBeads data set were collected using the 320/225 kV Nikon XTEK Bay at the Manchester X-ray Imaging Facility (MXIF), the University of Manchester. The apparatus consists of a cone-beam microfocus X-ray source that projects polychromatic X-rays onto a 2000 × 2000 pixel-length and width, 16-bit flat detector panel. The optimal window size for the SophiaBeads reconstructions is 1564 × 1564, see [7].

There are two samples (henceforth referred to as S1 and S2) that were scanned using the framework described in [6], and both samples comprised a plastic tube with a diameter of 25mm, filled with uniform Soda-Lime Glass (SiO<sub>2</sub>-Na<sub>2</sub>O) beads of diameters 2.5mm (S1) and 1.0mm (S2). S1 is publicly available; S2 on request. Here, we use S1 and S2 to represent different sparsity levels: the smaller beads of S2 have relatively more boundary pixels, which equates to more non-zero pixels in the gradient, and hence is less sparse than S1.

The present study uses a single central row of the 3D cone-beam data, and a 2D fan-beam geometry. For the constant-exposure series, the available data sets labelled 64-, 128-, 256-, 512- and 1024-projection are used. For the reduced-exposure series the 1024-projection data set is downsampled by repeatedly halving the number of projections while keeping every other one, thereby preserving the equiangular distribution.

B. Determining a ground truth image and its sparsity

The SophiaBeads data set is designed with fixed total exposure ranging from few high-exposure projections to many low-exposure projections. No high-quality data set (many high-exposure projections) is provided for the construction of a ground truth. However, each data set is recorded at slightly offset angular positions and we obtain a ground truth by pooling all projections for each of S1 and S2 and reconstruct using 30 iterations of the Conjugate Gradient Least Squares (CGLS) algorithm, followed by median filtering with a 5 × 5 filter to reduce noise. The resulting S1 and S2 ground truths are shown in full and close-up in Fig. 1.

To determine gradient sparsity of the ground truth images we count only nonzero gradient magnitude values greater than a threshold chosen empirically to preserve only bead edges and not noise. Thresholded gradient magnitude images are shown in Fig. 1. The S1 ground truth has 54543 nonzero values in its gradient, corresponding to a sparsity level (relative to the total number of pixels) of 54543/1564<sup>2</sup> = 2.2%. The same numbers for S2 are 123870 and 5.1%. This quantifies the

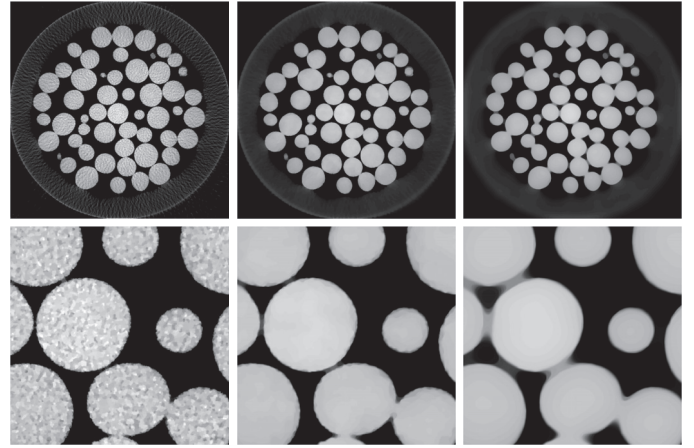


Fig. 2. TV-regularized reconstructions using regularization parameters 10<sup>-3</sup>, 10<sup>-2</sup> and 10<sup>-1</sup> (left to right). Full 1564 × 1564 images (top row) and 350 × 350 region of interest around the center (bottom row).

intuition that S1 is more gradient-sparse than S2, though exact numbers may vary depending on thresholds chosen.

III. RECONSTRUCTION PROBLEM AND ALGORITHM

A. Total variation optimization problem

We denote the log-transformed projection data by  $b$ , the 2D fan-beam system matrix by  $A$ , an image such as a reconstruction by  $u$ , in particular a TV-regularized solution by  $u_{TV}$ , and the number of projections by  $N_\theta$ . To determine a TV-regularized reconstruction (which can be seen as the maximum a posteriori estimate in a Bayesian formulation) of the discrete imaging model  $Au = b$  we solve the optimization problem

$$u_{TV} = \arg \min_u \frac{1}{2N_\theta} \|Au - b\|_2^2 + \alpha T_\tau(u), \quad u \geq 0, \quad (1)$$

where we employ a standard Huber-smoothed TV defined as

$$T_\tau(u) = \sum_j \Phi_\tau(\|D_j u\|_2), \quad \text{where} \quad (2)$$

$$\Phi_\tau(z) = \begin{cases} |z| - \frac{1}{2}\tau & \text{if } |z| \geq \tau, \\ \frac{1}{2\tau} z^2 & \text{else.} \end{cases} \quad (3)$$

Here,  $\alpha$  is the TV regularization parameter,  $D_j$  is a finite difference approximation to the gradient at pixel  $j$  and  $\|\cdot\|_2$  denotes the vector 2-norm (or Euclidian norm).

Smoothing is used to make the problem solvable by smooth optimization techniques which are generally faster than their non-smooth counterparts. Depending on the choice of smoothing parameter,  $\tau$ , this might modify the reconstruction; however here we use a sufficiently small value of  $\tau = 10^{-5}$  relative to the image values that smoothing effects are negligible.

Non-negativity is enforced as the object's attenuation coefficients are known to be non-negative and in general non-negativity can lead to substantial reconstruction improvement.

The normalization by  $N_\theta$  helps to compare reconstructions obtained at different  $N_\theta$  by compensating the magnitude of the first term which is otherwise proportional to  $N_\theta$ . As a result, a fixed  $\alpha$  value yields the same balance between the two terms

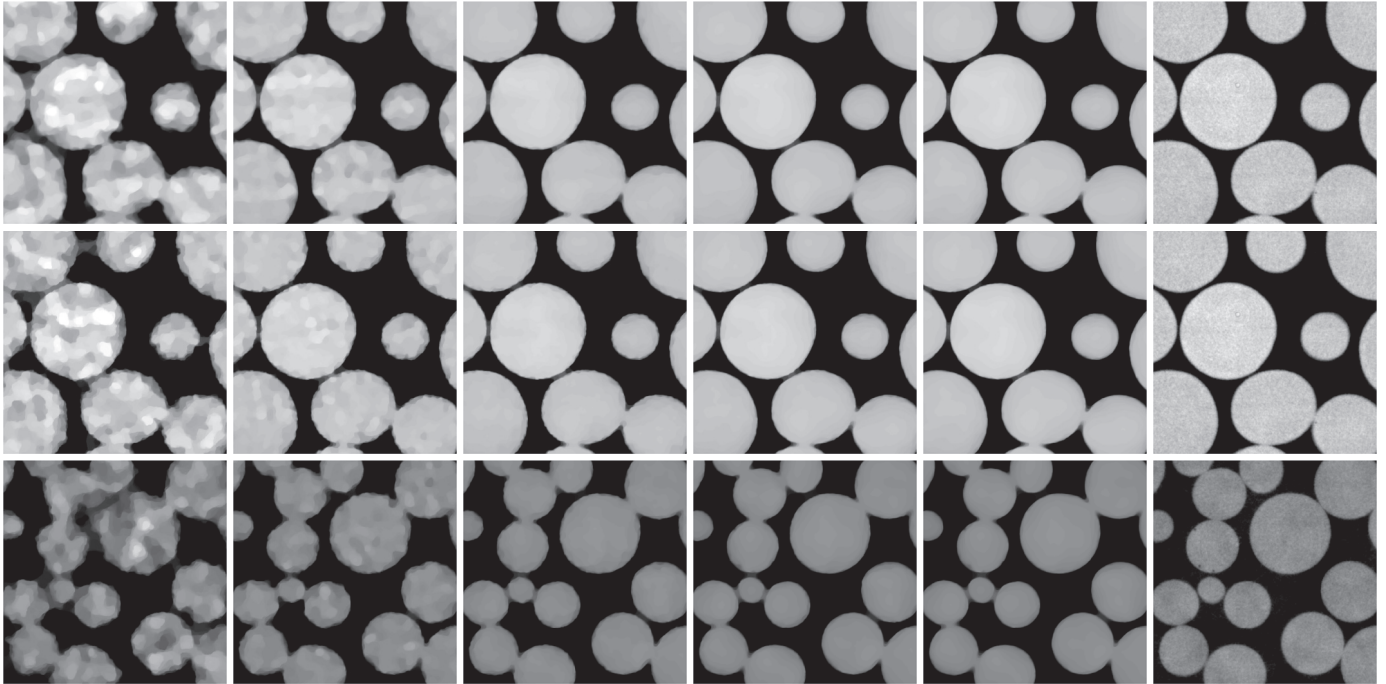


Fig. 3. TV-regularized reconstructions of 64-, 128-, 256-, 512-, 1024-projection data sets and pooled-data ground truths (left to right), showing a  $350 \times 350$ -pixel region of interest. S1 data set of fixed total exposure (top row), S1 and S2 data sets with fixed per-projection exposure (middle and bottom rows).

at different  $N_\theta$ . This reduces the search for the optimal  $\alpha$  to a single initial sweep, the resulting  $\alpha$  of which can be reused. In practice we verified this through  $\alpha$  sweeps at different  $N_\theta$  but for brevity have not included results here.

### B. High-accuracy optimization algorithm

To solve (1) we used the toolbox TVReg [8], which offers implementations (written in C with MATLAB interface) of accelerated gradient projection methods; specifically we used the provided GPBB (Gradient Projection Barzilai-Borwein) method which among other techniques employ acceleration in form of the Barzilai-Borwein step-size selection. To further accelerate the reconstruction, we employed the ASTRA Tomography Toolbox [9] for GPU-acceleration of the computationally expensive forward and back-projection operators.

We emphasize that our goal here is not necessarily to use the fastest algorithm but one that can reliably solve (1) to high accuracy in reasonable time in order that we indeed assess the quality of the TV-regularized reconstruction and not of an arbitrary early-termination result. TVReg is capable of this through a non-heuristic termination criterion based on the gradient norm magnitude, in contrast to, for example, running a pre-set fixed number of iterations or terminating when a small difference between iterates is encountered.

## IV. RESULTS

### A. Choosing the regularization parameter

Fig. 2 shows reconstructions for  $\alpha = 10^{-3}$ ,  $10^{-2}$  and  $10^{-1}$  showing the well-known transition from an under-regularized noisy/patchy TV-regularized reconstruction, through to an

over-regularized solution where separated beads appear connected due to excessive smoothing. Among a range of values we found  $\alpha = 10^{-2}$  to provide the best trade-off and this fixed value was reused in the remaining reconstructions.

### B. Assessment of reconstruction image quality

We assess the reconstructions qualitatively through visual inspection. For quantitative assessment we use two error measures with respect to the constructed ground truth  $u_{GT}$ : First, the standard relative 2-norm of pixelwise differences:  $E_1(u_{TV}) = \|u_{TV} - u_{GT}\|_2 / \|u_{GT}\|_2$ , where  $\|\cdot\|_2$  denotes the (Euclidian) 2-norm. The relative 2-norm provides a standardized comparison but is not necessarily the most informative about whether important features have been reliably reconstructed. For the second error measure  $E_2(u_{TV})$ , we evaluate the aspect ratio (width:height) of 25 reconstructed beads and report the mean relative error with respect to determined aspect ratios of the ground truth beads. This measure describes how well bead reconstructions reproduce the known bead shapes.

### C. Q1: Is it better to collect few high-exposure or many low-exposure projections?

We first address Q1 by determining the TV-regularized reconstruction of the fixed total exposure S1 data set for 64, 128, 256, 512 and 1024 projections. We visually compare a  $350 \times 350$ -pixel region of interest of all reconstructions with the constructed ground truth in the top row of Fig. 3. Visual quality clearly improves with increasing number of projections.

The error measures  $E_1$  and  $E_2$  are plotted in Fig. 4 using a full line. Both error measures agree with visual assessment that

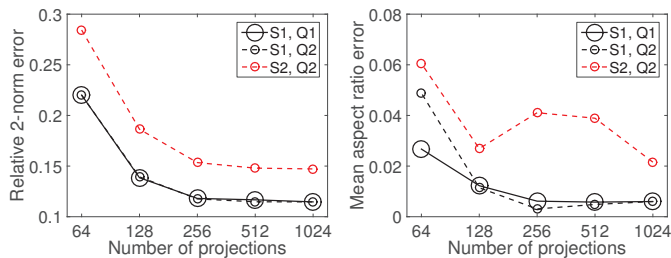


Fig. 4. Relative 2-norm error (left) and mean aspect ratio error (right) for data sets S1 and S2 with fixed total or per-projection exposure, Q1 and Q2.

the 64-projection reconstruction is substantially worse than the others and that error decays with more projections.

#### D. Q2: What is the dependence on sparsity?

To address Q2 the middle and bottom rows of Fig. 3 show reconstructions for the case of fixed exposure-per-projection for data sets S1 and S2. Corresponding error measures are plotted in Fig. 4 using dashed lines. First, again a clear trend of improved TV-regularized reconstruction quality with increasing number of projections is observed. This is less surprising than in the previous case, since more projections correspond to a higher X-ray exposure. However, for S2 the mean aspect ratio error for 256 and 512 projections is larger than the general trend. We also note that  $E_1$  for S1 in this case almost coincides with the fixed total exposure case.

In case the gradient sparsity does in fact affect the number of projections sufficient for accurate reconstruction, we would expect to see clear differences between S1 and the more gradient-sparse S2 data set. However, visually the S1 and S2 reconstructions show no clear difference in their dependence on the number of projections. The error plots also do not reveal clearly different behavior of S1 and S2 as function of numbers of projections, apart from the previously mentioned  $E_2$  values for S2 at 256 and 512 projections.

## V. DISCUSSION AND CONCLUSIONS

In all considered cases the 64-projection reconstructions stand out from the rest as substantially poorer. It seems that artifacts caused by having only 64 projections cannot be effectively removed by TV-regularized reconstruction, no matter whether high- or low-exposure projections are used. This is particularly interesting considering the highly gradient-sparse and round, piece-wise flat regions, for which TV-regularized reconstruction could be expected to excel.

For Q1, we conclude that given a fixed total exposure it appears beneficial to distribute across the highest possible number of projections. Even though each projection is of low quality it appears intuitively sensible to aim for obtaining in a loose sense more independent information about the scanned sample through more projection angles, rather than few high-quality ones. This is however in contrast to the typical message from the sparsity-regularization literature, namely that reconstruction from few projections is possible.

Regarding a possible connection to sparsity in Q2, present results are inconclusive since no clear difference is observed between S1 and S2. However for both S1 and S2 results, there is a large error reduction between 64 and 128 projections. This may hint that there is a number of projections, possibly different for each of S1 and S2, below which TV-regularized reconstruction will not be successful. The SophiaBeads data set only allows subsampling by factors of 2 to preserve equiangular projections. Relevant future work includes the acquisition and analysis of data sets with finer increments of numbers of projections, as well as more sparsity levels.

It should be mentioned that the presented preliminary conclusions may depend on several aspects of the study. For example it is unclear if the pooling approach produces a reliable enough ground truth, and in potential future work, extra care should be taken to acquire ground truth data. Also it is not certain that the error measures used here are the most informative and other options could be considered.

Lastly, regarding how SophiaBeads data sets serve as sparsity-regularization test data, we found TV-regularized reconstruction to work well on the piecewise constant bead images. In that sense, SophiaBeads is quite useful. However for assessing the influence of gradient sparsity we faced shortcomings which we have offered suggestions to address in future work.

## ACKNOWLEDGMENTS

The work by JSJ was supported by the project ‘‘High-Definition Tomography’’ funded by Advanced Grant No. 291405 from the European Research Council. The work by SBC was supported by the School of Mathematics (UoM), EPSRC CCPi (EP/J010456/1), and BP through the BP International Centre for Advanced Materials (BP-ICAM). Authors would also like to acknowledge the support of Samuel A. McDonald (MXIF) and EU COST action MP1207 (EXTREMA).

## REFERENCES

- [1] L. I. Rudin, S. Osher, and E. Fatemi, ‘‘Nonlinear total variation based noise removal algorithms,’’ *Physica D*, vol. 60, pp. 259–268, 1992.
- [2] J. Bian, J. H. Siewerdsen, X. Han, E. Y. Sidky, J. L. Prince, C. A. Pelizzari, and X. Pan, ‘‘Evaluation of sparse-view reconstruction from flat-panel-detector cone-beam CT,’’ *Phys Med Biol*, vol. 55, pp. 6575–6599, 2010.
- [3] J. S. Jørgensen and E. Y. Sidky, ‘‘How little data is enough? Phase-diagram analysis of sparsity-regularized X-ray computed tomography,’’ *Philos Trans R Soc Lond Ser A*, vol. 373, p. 20140387, 2015.
- [4] E. J. Candès, J. Romberg, and T. Tao, ‘‘Robust uncertainty principles: Exact signal reconstruction from highly incomplete frequency information,’’ *IEEE Trans Inf Theory*, vol. 52, pp. 489–509, 2006.
- [5] S. B. Coban and S. A. McDonald, ‘‘SophiaBeads Dataset Project,’’ Tech. Rep., 2015. [Online]. Available: <http://dx.doi.org/10.5281/zenodo.16474>
- [6] S. B. Coban, P. J. Withers, W. R. B. Lionheart, and S. A. McDonald, ‘‘When do iterative reconstruction methods become worth the effort?’’ in *Proc Fully3D*, Newport, RI, USA, 2015.
- [7] S. B. Coban, ‘‘SophiaBeads Dataset Project Codes,’’ 2015. [Online]. Available: <http://dx.doi.org/10.5281/zenodo.16539>
- [8] T. L. Jensen, J. H. Jørgensen, P. C. Hansen, and S. H. Jensen, ‘‘Implementation of an optimal first-order method for strongly convex total variation regularization,’’ *BIT*, vol. 52, pp. 329–356, 2012.
- [9] W. van Aarle, W. J. Palenstijn, J. De Beenhouwer, T. Altantzis, S. Bals, K. J. Batenburg, and J. Sijbers, ‘‘The ASTRA Toolbox: A platform for advanced algorithm development in electron tomography,’’ *Ultramicroscopy*, vol. 157, pp. 35–47, 2015.